PAPER

Sub-bandgap photoluminescence properties of multilayer h-BN-on-sapphire

To cite this article: Shantanu Saha *et al* 2022 *Nanotechnology* **33** 215702

View the article online for updates and enhancements.

Sub-bandgap photoluminescence properties of multilayer h-BN-on-sapphire

Shantanu Saha[1], **Yu-Chen Chang**[2], **Tilo Hongwei Yang**[2], **Anthony Rice**[3],
Arnob Ghosh[1], **Weicheng You**[1], **Mary Crawford**[3], **Ting-Hua Lu**[2] ⬤,
Yann-Wen Lan[2] **and Shamsul Arafin**[1] ⬤

[1] Department of Electrical and Computer Engineering, The Ohio State University, Columbus, OH 43210, United States of America
[2] Department of Physics, National Taiwan Normal University, Taipei 116, Taiwan
[3] Sandia National Laboratories, PO Box 5800, Albuquerque, NM 87185, United States of America

E-mail: arafin.1@osu.edu

Abstract

Two-dimensional hexagonal boron nitride (h-BN) materials have garnered increasing attention due to its ability of hosting intrinsic quantum point defects. This paper presents a photoluminescence (PL) mapping study related to sub-bandgap-level emission in bulk-like multilayer h-BN films. Spatial PL intensity distributions were carefully analyzed with 500 nm spatial resolution in terms of zero phonon line (ZPL) and phonon sideband (PSB) emission-peaks and their linewidths, thereby identifying the potential quantum point defects within the films. Two types of ZPL and PSB emissions were confirmed from the point defects located at the non-edge and edge of the films. Our statistical PL data from the non-edge- and edge-areas of the sample consistently reveal broad and narrow emissions, respectively. The measured optical properties of these defects and the associated ZPL peak shift and line broadening as a function of temperature between 77° and 300° K are qualitatively and quantitatively explained. Moreover, an enhancement of the photostable PL emission by at least a factor of $\times 3$ is observed when our pristine h-BN was irradiated with a 532 nm laser.

Keywords: h-BN, zero phonon line, photoluminescence, single photon emission, dangling bond, quantum point defects

(Some figures may appear in colour only in the online journal)

1. Introduction

Van der Waals (vdW) materials have enabled unprecedented scientific and technological breakthroughs in quantum information technologies and integrated quantum photonics. Among them, ultrawide bandgap h-BN is a promising frontrunner vdW host material of active quantum point defects, leading to single photon emitters (SPEs). Color centers in h-BN have generated interest in fundamental research to understand the potential of this material. As a good host of quantum point defects emitting from ultraviolet to near-infrared (IR), h-BN is a versatile material to be used for both optoelectronic and quantum devices [1]. Hence, comprehensive understanding of the basic optical properties of defects and controlling their

emission allow them to be used effectively in quantum technologies.

Emission properties of h-BN using sub-bandgap optical excitation is interesting for advancing the use of this vdW material in quantum nanophotonics [2]. Additionally, a sub-bandgap luminescence study of h-BN show emission from native defects or impurities while avoiding excitonic emissions [3]. In order to utilize these defect sources for the implementation of SPEs, clear understanding of their associated processes that give rise to quantum emission is essential [4]. These SPEs possess a series of ZPLs spanning a narrow or wide spectrum based on single or ensembled defects. Broad ZPL distributions are likely the result of the incorporation of multiple defects during h-BN growth [5]. In this study, we

1

report two different types of defects lying across the non-edge and edge of multilayer h-BN. Defects at, in particular, the film edge is promising as they not only change the local atomic structure but also engineer the electronic structure with controllable properties to yield stable quantum emission [6]. Investigation of the optical properties of such defects and their comparative analysis are, therefore, of great interest.

Optical properties of monolayer h-BN are significantly different from their bulk counterparts, rendering interesting phenomena such as spin-valley splitting and exciton phonon interactions [7]. To address defects hosted by h-BN, sub-bandgap optical studies were conducted and the emission wavelengths were varied by changing defect density, types and layer thickness. More than 85% of the reported emitters using the epitaxially-grown and exfoliated h-BN materials showed ZPL wavelengths at ∼580 nm [8–10]. Despite of low extraction efficiency and difficulty in controlling the position of emitters within the lattice, the emitters in multilayer h-BN were found to be with narrower emission lines than mono-layer h-BN [2] and both thermally-and optically-stable [11]. It is true that multilayer h-BN films exhibited both narrow and broad ZPL distributions depending upon the density of defects [5]. The SPEs based on h-BN multilayers emitting a broad range of wavelengths from UV to near IR were also reported [12]. Hence, multilayer h-BN defects are considered as attractive sources of single photon emission [13].

Motivated by the presence of point defects in h-BN and the recent works on isolated individual defects that emit single photons, a systematic and detailed experimental study of multilayer h-BN films using sub-bandgap photo-luminescence is conducted in this work. We first ensured the location of the defects by careful PL mapping of the entire h-BN film area which reveals the bright emission. PL measurements of the defects found across both the edge- and non-edges of the films were then investigated. Temperature dependent PL studies were then carried out to characterize peak wavelengths, lineshapes and intensity of the spectral emission. This survey reveals broad spectral features of an inhomogeneous distribution of ZPL and PSB across wide wavelength ranges, spanning between 570–610 nm and 620–650 nm, respectively.

2. Experimental details

Borazine, a carbon free precursor, was used during wafer-scale growth of h-BN films using chemical vapor deposition. Growth details of multilayer h-BN used in the study can be found elsewhere [14, 15]. The schematic diagram and Nomarski microscope image of as-grown multilayer h-BN-on-sapphire is shown in figures 1(a) and (b), respectively. The chemical structure of the resulting films was first analyzed using a Kratos Axis Ultra x-ray photoelectron spectroscopy (XPS) instrument. The XPS survey spectrum of the as-grown films is presented in figure 1(c). The material XPS analysis in terms of high-resolution spectrum for C 1s, B 1s and N 1s were presented in [15]. Note that a very weak 284.5 eV carbon peak was also observed despite the use of a carbon-free precursor, suggesting the
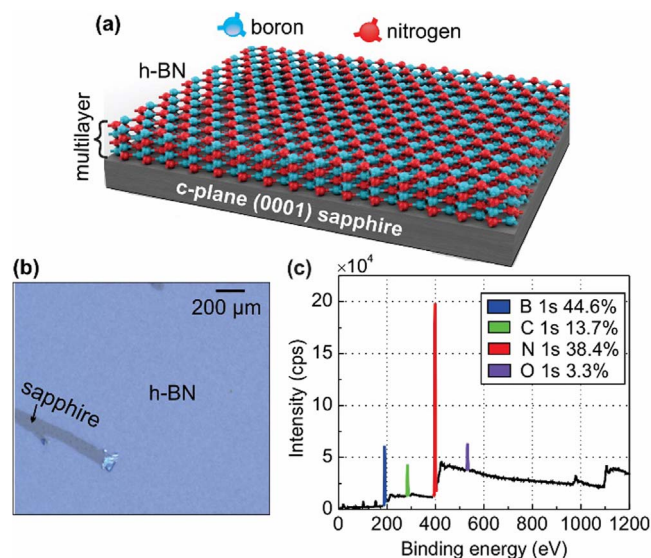

Figure 1. (a) Schematic diagram of multilayer 2D h-BN thin films grown on c-plane sapphire substrates, (b) NoMarski microscopy image of the sample with films scrapped off at the edge to obtain a visual contrast and (c) XPS spectrum with various peaks related to B, N, C and O atoms in the film.

presence of adventitious carbon atoms. This may originate due to the material exposure to ambient air before introduction into the spectrometer. Such low (13%) value of carbon may also result from sample preparation, handling or from other sources of ambient. A very weak O 1s peak was also found at 532.9 eV [16].

PL mapping was carried out on irregularly shaped h-BN flakes which were obtained by mechanically deforming the as-grown materials. Although our as-grown h-BN on a 2′ diameter sapphire was a large-area film, we deliberately made this material to be a smaller piece in order to obtain film edges. The deformed flake-like h-BN material, as shown in figure 2(a), provides 'edge'-induced defects in addition to random point defects which are termed as 'non-edge' defects in our paper. A 532 nm green laser with 6 mW continuous-wave (CW) excitation power was used to map a number of spots resulting from individual and small clusters of color centers in the h-BN flake. A confocal microscopic PL system, possessing piezoelectric XYZ scanners with a spatial resolution of about 500 nm, was employed for PL mapping. The light beam was focused through a $100 \times$ objective to a spot size of 1 μm. Spectra were collected by an ANDOR spectrometer (model: Kymera 328i) with an imaging source CCD camera (model: DFK 33UP5000). High-resolution spectra were acquired using a 1200 lines mm^{-1} grating and 5 s integration time. A Semrock long-pass filter (BLP01-532R-25) was used to reduce the residual excitation beam. The selected wavelength windows were 580–600 nm for ZPL and 620–640 nm for PSB.

3. Results and analysis

Spatially resolved PL images reveal the luminescence occurring from the ZPL and the PSB of the sample as shown
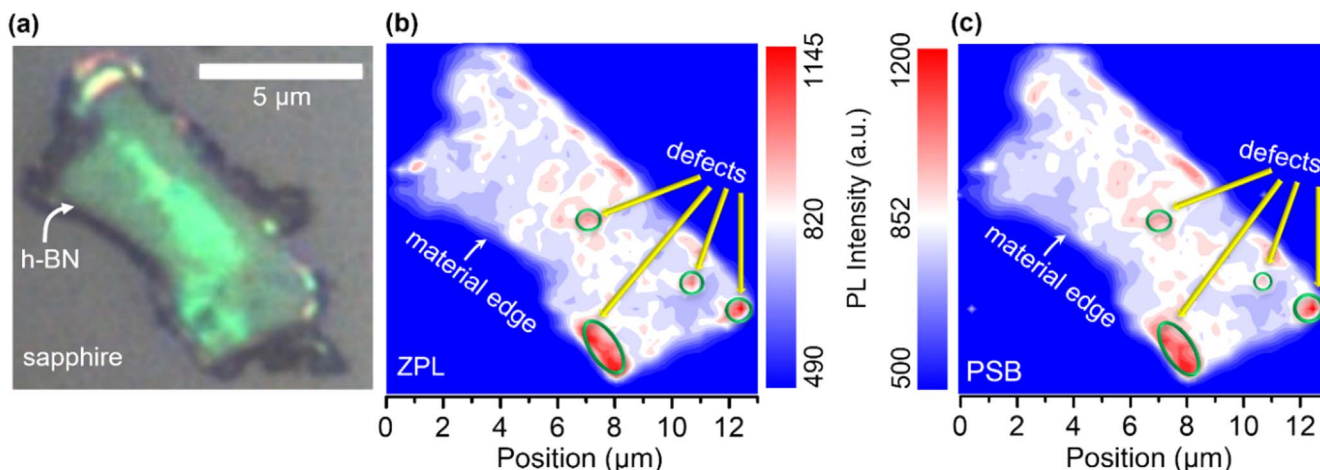
Figure 2. (a) Optical microscope image of the as-grown flake-like h-BN sample, spatial PL mapping data of h-BN for (b) ZPL and (c) PSB emissions, revealing the quantum point defects.

in figures 2(b) and (c), respectively. The representative defects are encircled and the red areas indicate relatively stronger emission compared to the rest of the flake area.

3.1. Room-temperature PL measurement

Impurities and native defects are present in bare sapphire substrates and therefore, it is important to distinguish whether the observed defects are from sapphire or the h-BN films. Interestingly, heating the substrates at the h-BN growth temperature modifies the substrate defect properties through the creation of new defects [17]. These defects at deep levels tend to have broad PL features induced by strong phonon interactions. Therefore, we first measured the PL spectrum of the heat-cycled sapphire substrates to help distinguish them from h-BN PL peaks. As-received sapphire from commercial vendors mostly shows the emission spectrum with Cr^{3+} peaks at 692.8 nm and 694.2 nm, while the sapphire heated at 1500 °C shows Cr^{3+} luminescence at 693.1 and 694.2 nm, as shown in figure 3(a). These measured data closely match the previously reported results obtained after the substrate was heated to 1650 °C [18]. Two additional small peaks at 706 nm and 713 nm are observed in the spectra, which possibly also originate from sapphire.

Measurements of room-temperature (RT) PL from h-BN under study elucidated the difference from sapphire induced emission. PL measurements of point defects, the 'non-edge' type was first studied. These defects could be spatially located anywhere inside the h-BN flakes. Figure 3(b) shows the RT PL spectrum of a representative non-edge h-BN defect. Considering the PL lineshapes and relative intensities, the broad ZPL emission at around 592 nm (=2.09 eV) and the PSB emission at 634 nm (=1.95 eV) are observed. The use of a carbon-free precursor tentatively implies that the origin of this emission is not likely due to carbon-based impurities (C-N, C-B). Instead this is most liekly caused by the native defects including nitrogen-vacancy (V_N), anti-site complex ($N_B V_N$), and any other intrinsic defects [3]. The exact origin of the defects responsible for the ZPL is beyond the scope of this work and will be investigated in our future studies. The

energy difference between ZPL and PSB was found to be 140 meV which corresponds to the in-plane longitudinal optical and transverse optical (LO/TO) phonon energy. This value is in good agreement with the previously reported values, i.e., 165 ± 10 meV [19].

Figure 3(c) presents the RT PL spectrum of a h-BN edge-defect. The peak around 596 nm (=2.08 eV) and 637 nm (=1.94 eV) are considered to be ZPL and PSB emissions, respectively, with a spectral separation of 130 meV. Boron dangling bonds are the likely origin of the observed ZPL and PSB emissions because the electronic structures of nitrogen dangling bonds do not yield emission around 2 eV [20, 21]. It has been experimentally confirmed that dangling-bond induced defects and the associated SPEs are mostly localized near grain boundaries or material edges [10, 22, 23]. Our measured ZPLs appear at 2.08 eV with a full width at half maximum (FWHM) of ~13 nm, which are consistent with the previous experimental observations [10, 22, 23]. This suggests the likelihood of the presence of boron dangling bonds at the edge of our h-BN. It should be noted that dangling bonds on material edges are prone to be bonded with electronegative atoms/radicals and may change the optical properties of the materials. In our case, boron-ended edges might terminate with ambient oxygen and may affect the optical properties of the materials. Identifying the chemical nature of the edges responsible for the emission shown in figure 3(c) requires further structural analysis using high resolutions transmission electron microscopy (HRTEM) and this will be investigated in our future studies.

One salient difference between the 'edge-' and 'non-edge' point defects is that the emission originates from the h-BN edge exhibits relatively narrower ZPL lineshapes compared to the non-edge type. This could be attributed to the presence of a higher defect density at the non-edge area compared to the edge-defects with possibly a lower density. Moreover, local lattice strain and dielectric environment are the other two potential factors which could explain the difference in the PL lineshapes [24].
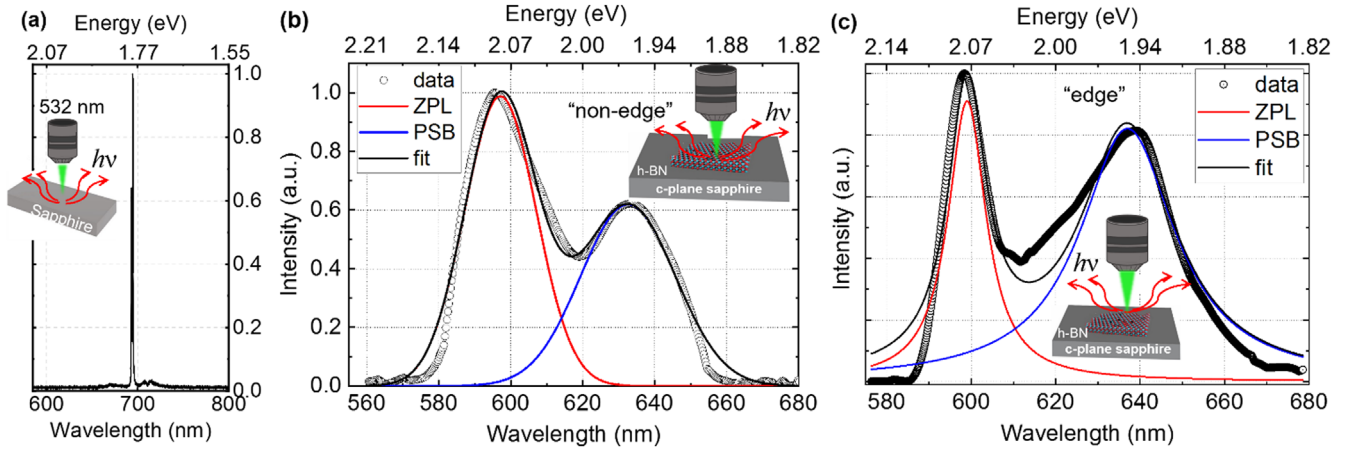
Figure 3. (a) Room-temperature PL emission from (a) sapphire substrates, (b) non-edge- and (c) edge-defects of multilayer as-grown h-BN.

The calculated Debye–Waller (DW) factor is defined as the ratio of integrated luminescence intensity of ZPL (I_{ZPL}) to the total integrated luminescence intensity (I_{total}), which clarifies the extent of electron and phonon coupling. The measured DW is found to be 0.54 from the non-edge area while the calculated value at edge is 0.35. These factors are close to the values where strong and narrow-linewidth ZPL emission from a single defect embedded in multilayer h-BN was reported [25]. Unfortunately, such low values may limit the efficiency of a spin-photon interface in quantum networks [26].

The PL spectra collected from non-edge and edge of the films are found to be different mainly in terms of the lineshape. To prove this not to be an occasional finding, statistical analysis of RT PL data was performed. PL area mapping was conducted once again at a number of h-BN locations near the non-edge and edge areas. Figure 4(a) shows the number of non-edge and edge-locations of the h-BN flake where PL was measured. Total 206 different spatial locations were probed. Only 63 locations were inside the dashed grey line, i.e., non-edge. The remaining 143 locations outside the dashed grey line, i.e. 'edge' area - show a ZPL at 592 ± 2 nm and a weaker second peak at 636 ± 2 nm. The slight wavelength variation in either '63-non-edge' or '143-edge' locations is probably due to the inhomogeneous broadening of several defect species within h-BN, its random orientation and arbitrary mechanical contact between h-BN and the underlying sapphire substrate [27]. In regard to PL lineshape, broader emission of ZPL and PSB were consistently found from the non-edge area as shown in figure 4(b) while figure 4(c) displays the narrower lines that were obtained from the edge area. This could be due to several reasons including the possibility of containing a higher defect density at the non-edge area. Moreover, broadening could also occur due to the presence of local lattice strain which leads to increased scattering between the energy levels of h-BN [28, 29]. The change in emission wavelengths and lineshapes may also result from inhomogeneous broadening of several defect species or can likely originate from defects belonging to the same atomistic model coupled to the fluctuating local lattice strain and/or dielectric environments [30].

3.2. Statistical analysis

3.2.1. Temperature-dependent PL measurement. To investigate the effect of temperature on the spectral properties of the point defects, temperature-dependent PL measurements were carried out. Figure 5(a) presents the PL emission spectra for a representative 'non-edge' defect. As expected, the PL intensity decreases with increasing temperature. The decrease in emission intensity is primarily caused by the increase in nonradiative transition rate because the initial state of the recombination process depopulates with increasing temperature [31]. To estimate the ZPL peak and FWHM values, the emission spectra for each temperature were fitted to a linear combination of a background and a Lorentzian line shape using

$$L(E) \alpha \frac{1}{(E - E_{ZPL})^2 + \left(\frac{\Gamma}{2}\right)^2},$$

where E_{ZPL} is the ZPL emission energy, Γ is the FWHM and $L(E)$ is proportional to the number of photons emitted in the energy range $(E, E + dE)$.

The energy peak position exhibits a red shift with increasing temperature as shown in figure 5(b). The increase in the bulk lattice constant and the electron-phonon interaction with increasing temperature causes such a red shift which is an intradefect optical transition [13]. Although our spectral redshift is in good agreement with the behavior reported using exfoliated h-BN [13], the amount of the ZPL peak shift over the measured temperature range is roughly a factor of ×2–3 smaller than our observation. This could be attributed to the presence of strain that developed during growth [14, 15]. The as-grown h-BN under study is likely to have more strain compared to an exfoliated one. The solid red line in figure 5(b) represents the fitting which show a $T^3 + T$ trend. In fact, the fitting was performed with the function, $AT^3 + BT$, where A and B are free parameters. The contribution from the electron-phonon interaction to the lineshift is realized via the piezoelectric coupling proportional to T and the deformation potential proportion to T^3. Hence the ZPL energy exhibits a strong dependence on temperature.
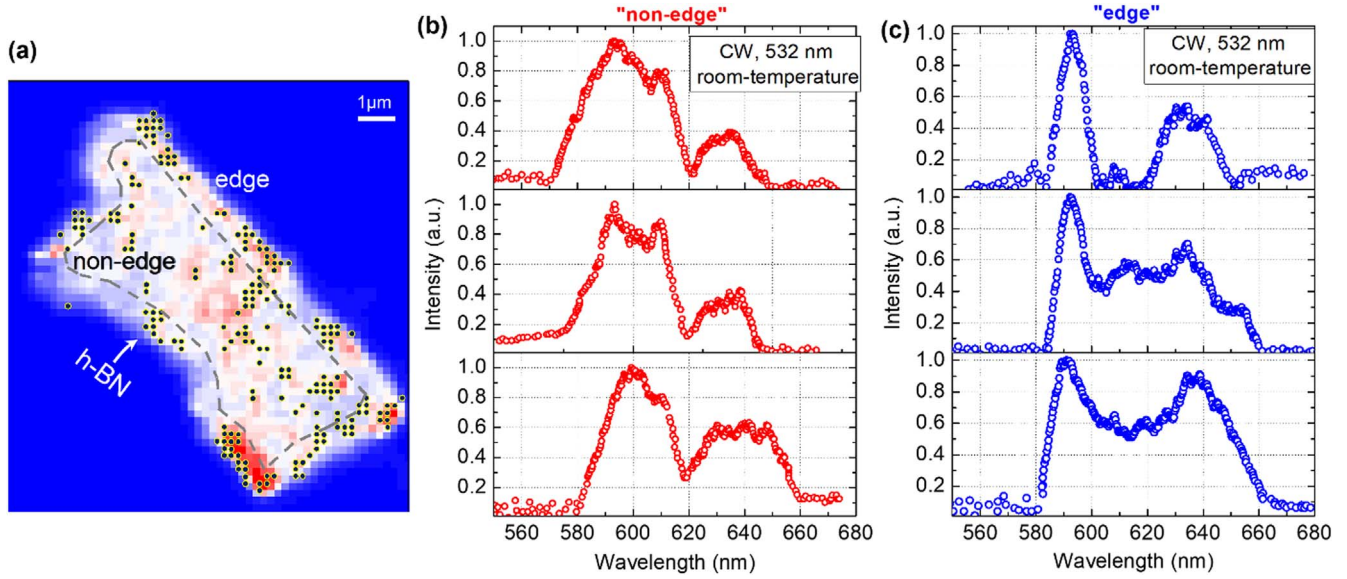
Figure 4. (a) PL mapping at different locations of h-BN, (b) statistical representation of broad ZPL and PSB across non-edge and (c) narrow ZPL and PSB across edge of the sample.
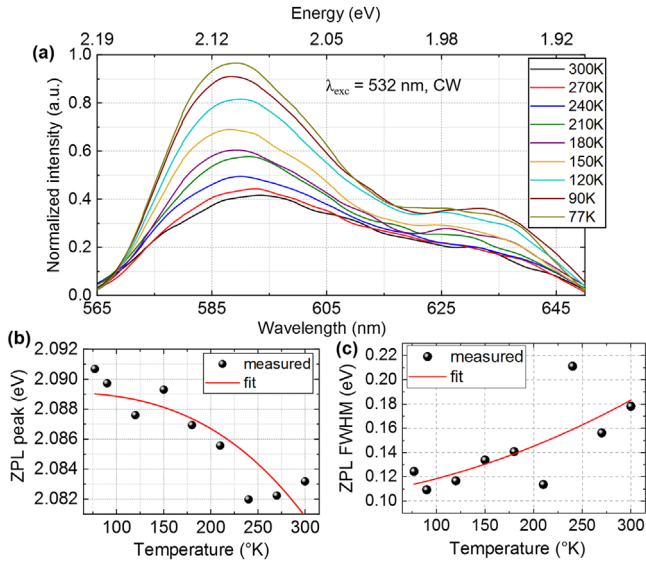

Figure 5. (a) Temperature-dependent PL emission, (b) red shift of the ZPL emission peak and (c) broadening of the ZPL emission linewidth with increasing temperature.

Similar to conventional semiconductors, FWHMs of defect-related spectra often increases with temperature. Considering FWHMs of ZPL emission at a given temperature, we observe a FWHM of 35 nm (113 meV) at 77 K. Interestingly, a FWHM of 0.25 nm (0.74 meV) at 77 K of a single point defect in multilayer h-BN was reported [2]. Our ZPL FWHM at RT is measured to be 57 nm (163 meV) which is much broader than the FWHMs of ZPL (10-35 nm = 36-130 meV) at RT and the associated defects causing the ZPL emission are claimed to be ensembled [5]. This suggests that the ZPL emission observed in this study caused by ensemble point defects. Moreover, the recently reported results [32] support the presence of ensemble point defects in our as-grown h-BN materials. The temperature dependence of ZPL FWHM of the ZPL was fitted by [33] and

indicated in figure 5(c) with the red-solid line.

$$\Gamma = \Gamma_{o}\sqrt{\coth\left(\frac{\hbar\omega_{o}}{k_{B}T}\right)},$$

where Γ_{o} is the linewidth at absolute zero temperature, $\hbar\omega_{o}$ the photon energy at absolute zero temperature and k_{B} the Boltzmann constant. Such strong dependence on temperature has also been observed in quantum dots [34] and defects in diamond [35]. The broadening of FWHM with increasing temperature from 77 K to 300 K was found to be approximately 60 meV, as shown in figure 5(c). This clearly indicates that temperature has much stronger dependence on the ZPL broadening compared to ZPL energy. Note that the measured FWHM change, i.e., 60 meV differs from the previously reported values ∼6 meV [13] and ∼12 meV [25]. This could be attributed to the presence of ensemble defects in our h-BN materials as opposed to the single defect in h-BN [13]. Additionally, the presence of strain prevalent to our h-BN also contributes to such spectral broadening [29].

3.3. Photostability measurement

One important issue, especially for the use of point defect-based emitters in applications, is the stability of the optical properties under continuous light irradiation. To explore the photostability, our pristine h-BN material was exposed to irradiation with a CW 532 nm laser for 1 h. Under a high excitation power of 6 mW (power density 7.6 mW μm^{-2}) roughly a factor of ×3 enhancement of PL signal with respect to the pristine h-BN is observed. No obvious change in the ZPL peak position with a slight change in PSB lineshape is observed, as shown in figure 6. The absence of PL bleaching and blinking during the measurement unveil the great potential of photostable emitters.

The PL spectral lineshape and intensity were also observed to change back to the pristine h-BN's case after the material was kept to ambient for some time, indicating that no
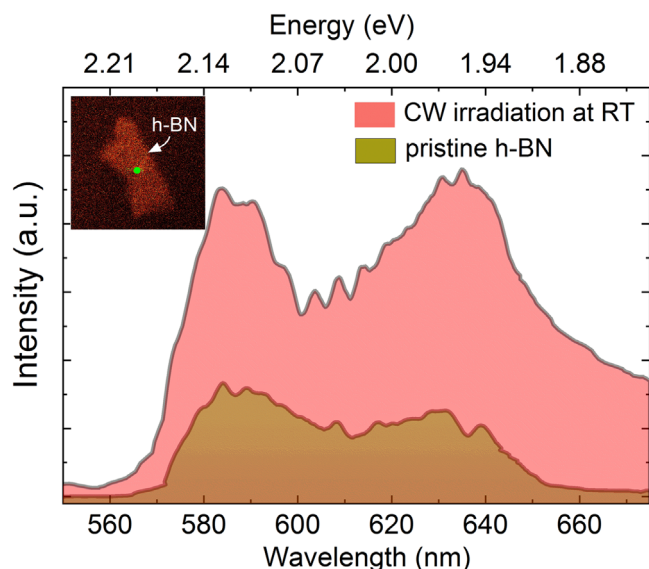
Figure 6. PL spectra of pristine h-BN and the material irradiated with a 532 nm laser for 1 h.

material degradation occurred during the illumination process. The reason of the temporary PL signal enhancement is not yet understood and requires further investigation. It could happen that the intensity of the background emission grows in time, when exposing the emitter with laser excitation for an extended period of time. Such long irradiation may also somehow clean the material surface by removing organic-based contaminants and water molecules on the material surface, which may cause the signal enhancement.

4. Conclusion

In conclusion, we investigate spatial distribution of defects and sub-bandgap optical properties of h-BN. The mapping study helped identify bright luminescence from various defects in the h-BN films. The PL measurements distinguished two types of quantum point defects and offered new insights into the optical properties of h-BN. The observed asymmetric broadening of ZPL emissions is probably due to the presence of ensemble defects. Boron dangling bonds are likely the cause for the 'edge'-induced defects. Consistent broad and narrow ZPL emission from non-edge and edge of the films support presence of two different types of defects in the film. Understanding the defect chemistry and identifying chemical species responsible for the 'non-edge' type defects and the resulting emission reported here are beyond the scope of this work and will be investigated in the future. Among native point defects, carbon is less likely due to the use of a carbon-free precursor during h-BN growth. Our next step is to grow few-defects h-BN films and introducing foreign atoms on top of such materials at particular spatial locations, being pivotal for the realization of deterministic quantum point defects. This is an essential step toward development and demonstration of robust and controllable SPEs that can be used for future quantum information processing technologies.

Data availability statement

All data that support the findings of this study are included within the article (and any supplementary files).

ORCID iDs

Ting-Hua Lu https://orcid.org/0000-0002-8803-5229
Shamsul Arafin https://orcid.org/0000-0003-4689-2625

References

[1] Khatri P, Ramsay A J, Malein R N E, Chong H M and Luxmoore I J 2020 Optical gating of photoluminescence from color centers in hexagonal boron nitride *Nano Lett.* **20** 4256–63
[2] Tran T T, Bray K, Ford M J, Toth M and Aharonovich I 2016 Quantum emission from hexagonal boron nitride monolayers *Nat. Nanotechnol.* **11** 37–41
[3] Weston L, Wickramaratne D, Mackoit M, Alkauskas A and Van de Walle C 2018 Native point defects and impurities in hexagonal boron nitride *Phys. Rev.* B **97** 214104
[4] Lyu C, Zhu Y, Gu P, Qiao J, Watanabe K, Taniguchi T and Ye Y 2020 Single-photon emission from two-dimensional hexagonal boron nitride annealed in a carbon-rich environment *Appl. Phys. Lett.* **117** 244002
[5] Mendelson N, Chugh D, Reimers J R, Cheng T S, Gottscholl A, Long H, Mellor C J, Zettl A, Dyakonov V and Beton P H 2021 Identifying carbon as the source of visible single-photon emission from hexagonal boron nitride *Nat. Mater.* **20** 321–8
[6] Zhang J, Sun R, Ruan D, Zhang M, Li Y, Zhang K, Cheng F, Wang Z and Wang Z-M 2020 Point defects in two-dimensional hexagonal boron nitride: a perspective *J. Appl. Phys.* **128** 100902
[7] Song L, Ci L, Lu H, Sorokin P B, Jin C, Ni J, Kvashnin A G, Kvashnin D G, Lou J and Yakobson B I 2010 Large scale growth and characterization of atomic hexagonal boron nitride layers *Nano Lett.* **10** 3209–15

[8] Mendelson N, Xu Z-Q, Tran T T, Kianinia M, Scott J, Bradac C, Aharonovich I and Toth M 2019 Engineering and tuning of quantum emitters in few-layer hexagonal boron nitride *ACS Nano* **13** 3132–40

[9] Stern H L, Wang R, Fan Y, Mizuta R, Stewart J C, Needham L-M, Roberts T D, Wai R, Ginsberg N S and Klenerman D 2019 Spectrally resolved photodynamics of individual emitters in large-area monolayers of hexagonal boron nitride *ACS Nano* **13** 4538–47

[10] Choi S, Tran T T, Elbadawi C, Lobo C, Wang X, Juodkazis S, Seniutinas G, Toth M and Aharonovich I 2016 Engineering and localization of quantum emitters in large hexagonal boron nitride layers *ACS Appl. Mater. Interfaces* **8** 29642–8

[11] Kianinia M, Regan B, Tawfik S A, Tran T T, Ford M J, Aharonovich I and Toth M 2017 Robust solid-state quantum system operating at 800 K *ACS Photonics* **4** 768–73

[12] Tran T T, Zachreson C, Berhane A M, Bray K, Sandstrom R G, Li L H, Taniguchi K, Watanabe K, Aharonovich I and Toth M 2016 Quantum emission from defects in single-crystalline hexagonal boron nitride *Phys. Rev. Appl.* **5** 034005

[13] Jungwirth N R, Calderon B, Ji Y, Spencer M G, Flatté M E and Fuchs G D 2016 Temperature dependence of wavelength selectable zero-phonon emission from single defects in hexagonal boron nitride *Nano Lett.* **16** 6052–7

[14] Rice A, Allerman A, Crawford M, Beechem T, Ohta T, Spataru C, Figiel J and Smith M 2018 Effects of deposition temperature and ammonia flow on metal-organic chemical vapor deposition of hexagonal boron nitride *J. Cryst. Growth* **485** 90–5

[15] Saha S *et al* 2021 Comprehensive characterization and analysis of hexagonal boron nitride on sapphire *AIP Adv.* **11** 055008

[16] Rastogi P K, Sahoo K R, Thakur P, Sharma R, Bawari S, Podila R and Narayanan T N 2019 Graphene–hBN non-van der Waals vertical heterostructures for four-electron oxygen reduction reaction *Phys. Chem. Chem. Phys.* **21** 3942–53

[17] Song Y, Zhang C, He D, Zhang L, Gou J, Yang Y and Li J 2012 Annealing effects on the photoluminescence of Pb-ion irradiated He-doped sapphire *Sci. China Phys., Mech. Astron.* **55** 1803–7

[18] Wanthanachaisaeng B, Bunnag N, Sutthirat C, Atichat W, Ounorn P, Sripoonjan T, Lenz C and Nasdala L 2013 Investigation of Be-treated sapphire by luminescence spectroscopy *Conference on Raman and Luminescence Spectroscopy (University of Vienna, Austria, July 3–6, 2013)*

[19] Tran T T, Elbadawi C, Totonjian D, Lobo C J, Grosso G, Moon H, Englund D R, Ford M J, Aharonovich I and Toth M 2016 Robust multicolor single photon emission from point defects in hexagonal boron nitride *ACS Nano* **10** 7331–8

[20] Turiansky M E and Van de Walle C G 2021 Boron dangling bonds in a monolayer of hexagonal boron nitride *J. Appl. Phys.* **129** 064301

[21] Turiansky M E, Alkauskas A, Bassett L C and Van de Walle C G 2019 Dangling bonds in hexagonal boron nitride as single-photon emitters *Phys. Rev. Lett.* **123** 127401

[22] Xu Z-Q, Elbadawi C, Tran T T, Kianinia M, Li X, Liu D, Hoffman T B, Nguyen M, Kim S and Edgar J H 2018 Single photon emission from plasma treated 2D hexagonal boron nitride *Nanoscale* **10** 7957–65

[23] Chejanovsky N, Rezai M, Paolucci F, Kim Y, Rendler T, Rouabeh W, Fávaro de Oliveira F, Herlinger P, Denisenko A and Yang S 2016 Structural attributes and photodynamics of visible spectrum quantum emitters in hexagonal boron nitride *Nano Lett.* **16** 7037–45

[24] Chakraborty C, Vamivakas N and Englund D 2019 Advances in quantum light emission from 2D materials *Nanophotonics* **8** 2017–32

[25] Ari O, Fırat V, Polat N, Cakir O and Ates S 2019 Influence of electron-phonon interactions on the spectral properties of defects in hexagonal boron nitride *Opt. Soc. Am.* **2** p S4A

[26] Atatüre M, Englund D, Vamivakas N, Lee S-Y and Wrachtrup J 2018 Material platforms for spin-based photonic quantum technologies *Nat. Rev. Mater.* **3** 38–51

[27] Lazić S *et al* 2019 Dynamically tuned non-classical light emission from atomic defects in hexagonal boron nitride *Commun. Phys.* **2** 113

[28] Mendelson N, Doherty M, Toth M, Aharonovich I and Tran T T 2020 Strain-induced modification of the optical characteristics of quantum emitters in hexagonal boron nitride *Adv. Mater.* **32** 1908316

[29] Li S, Chou J-P, Hu A, Plenio M B, Udvarhelyi P, Thiering G, Abdi M and Gali A 2020 Giant shift upon strain on the fluorescence spectrum of VNNB color centers in h-BN *npj Quantum Inf.* **6** 1–7

[30] Grosso G, Moon H, Lienhard B, Ali S, Efetov D K, Furchi M M, Jarillo-Herrero P, Ford M J, Aharonovich I and Englund D 2017 Tunable and high-purity room temperature single-photon emission from atomic defects in hexagonal boron nitride *Nat. Commun.* **8** 705

[31] Koperski M, Vaclavkova D, Watanabe K, Taniguchi T, Novoselov K S and Potemski M 2020 Midgap radiative centers in carbon-enriched hexagonal boron nitride *Proc. Natl Acad. Sci.* **117** 13214–9

[32] Stern H L, Jarman J, Gu Q, Barker S E, Mendelson N, Chugh D, Schott S, Tan H H, Sirringhaus H and Aharonovich I 2022 Room-temperature optically detected magnetic resonance of single defects in hexagonal boron nitride *Nat. Commun.* **13** 1–9

[33] Alkauskas A, McCluskey M D and Van de Walle C G 2016 Tutorial: defects in semiconductors—combining experiment and theory *J. Appl. Phys.* **119** 181101

[34] Favero I, Berthelot A, Cassabois G, Voisin C, Delalande C, Roussignol P, Ferreira R and Gérard J-M 2007 Temperature dependence of the zero-phonon linewidth in quantum dots: an effect of the fluctuating environment *Phys. Rev.* B **75** 073308

[35] Hizhnyakov V, Kaasik H and Sildos I 2002 Zero-phonon lines: the effect of a strong softening of elastic springs in the excited state *Phys. Status Solidi* b **234** 644–53